

Runx2 Regulates Mouse Tooth Root Development Via Activation of WNT Inhibitor NOTUM

Quan Wen,^{1,2} Junjun Jing,¹ Xia Han,¹ Jifan Feng,¹ Yuan Yuan,¹ Yuanyuan Ma,¹ Shuo Chen,¹ Thach-Vu Ho,¹ and Yang Chai¹ 

¹Center for Craniofacial Molecular Biology, University of Southern California (USC), Los Angeles, CA, USA

²Peking University Hospital of Stomatology First Clinical Division, Beijing, China

ABSTRACT

Progenitor cells are crucial in controlling organ morphogenesis. Tooth development is a well-established model for investigating the molecular and cellular mechanisms that regulate organogenesis. Despite advances in our understanding of how tooth crown formation is regulated, we have limited understanding of tooth root development. Runt-related transcription factor 2 (RUNX2) is a well-known transcription factor in osteogenic differentiation and early tooth development. However, the function of RUNX2 during tooth root formation remains unknown. We revealed in this study that RUNX2 is expressed in a subpopulation of GLI1+ root progenitor cells, and that loss of *Runx2* in these GLI1+ progenitor cells and their progeny results in root developmental defects. Our results provide *in vivo* evidence that *Runx2* plays a crucial role in tooth root development and in regulating the differentiation of root progenitor cells. Furthermore, we identified that *Gli1*, *Pcp4*, *NOTUM*, and *Sfrp2* are downstream targets of *Runx2* by integrating bulk and single-cell RNA sequencing analyses. Specifically, ablation of *Runx2* results in downregulation of WNT inhibitor *NOTUM* and upregulation of canonical WNT signaling in the odontoblastic site, which disturbs normal odontoblastic differentiation. Significantly, exogenous NOTUM partially rescues the impaired root development in *Runx2* mutant molars. Collectively, our studies elucidate how *Runx2* achieves functional specificity in regulating the development of diverse organs and yields new insights into the network that regulates tooth root development. © 2020 The Authors. *Journal of Bone and Mineral Research* published by Wiley Periodicals LLC on behalf of American Society for Bone and Mineral Research (ASBMR).

KEY WORDS: *Gli1*; *NOTUM*; ROOT DEVELOPMENT; *Runx2*; WNT/ β -CATENIN

Introduction

Teeth perform extensive functions in our daily lives, not only by participating in crucial physiological processes such as mastication, but also by contributing significantly to the aesthetics of the craniofacial complex. Teeth are composed of two major parts, the crown and the root. The crown is the visible component in the oral cavity, whereas the root extends into the jawbone and integrates our dentition with mandible and maxilla. Similar to how most ectodermal organs develop, tooth morphogenesis involves a sequence of reciprocal inductive molecular interactions between dental epithelium and underlying cranial neural crest–derived ectomesenchymal cells.^(1,2)

It has long been recognized that the tooth provides an excellent model for studying the regulation of organogenesis. The regulatory network that governs tooth crown development has been

extensively studied,^(3–5) but the regulatory mechanism of root development remains largely unknown. Studies have shown that major signaling pathways, such as TGF- β , BMP, FGF, WNT, sonic hedgehog (SHH), and PTHrP/parathyroid hormone 1 receptor (PTH1R) participate in root development,^(6,7) but it is not yet known how these signals achieve their functional specificity in root development. It is plausible that a network of transcription factors may play a crucial role in this process.⁽⁸⁾

Runt-related transcription factor 2 (RUNX2) is well known for its regulatory role in osteogenesis and tooth development. It is indispensable for mesenchymal progenitor cells' commitment to the osteoblastic lineage and also modulates their proliferation, differentiation, and maintenance.⁽⁹⁾ In humans, *RUNX2* mutations can cause an autosomal dominant syndrome, cleidocranial dysplasia (CCD), which affects the bones and teeth and is characterized by short

This is an open access article under the terms of the Creative Commons Attribution-NonCommercial-NoDerivs License, which permits use and distribution in any medium, provided the original work is properly cited, the use is non-commercial and no modifications or adaptations are made.

Received in original form March 21, 2020; revised form June 15, 2020; accepted June 17, 2020. Accepted manuscript online June 22, 2020.

Address correspondence to: Yang Chai, DDS, PhD, Center for Craniofacial Molecular Biology, University of Southern California, 2250 Alcazar Street – CSA 103, Los Angeles, CA 90033, USA. E-mail: ychai@usc.edu

Additional Supporting Information may be found in the online version of this article.

Journal of Bone and Mineral Research, Vol. 35, No. 11, November 2020, pp 2252–2264.

DOI: 10.1002/jbmr.4120

© 2020 The Authors. *Journal of Bone and Mineral Research* published by Wiley Periodicals LLC on behalf of American Society for Bone and Mineral Research (ASBMR).

stature, delayed cranial suture closure, abnormal clavicle formation, and dental anomalies, including delayed tooth eruption and supernumerary teeth.⁽¹⁰⁾ The dental anomalies in CCD patients suggest the importance of RUNX2 in tooth formation and eruption, but no root defect has been reported in these patients. Several studies using animal models have revealed that *Runx2* is required for early tooth development. *Runx2*-deficient mice exhibit arrested molar and incisor development at the early cap stage.⁽¹¹⁾ Ablation of *Runx2* in dental epithelium using *K14-cre* suppresses enamel maturation.⁽¹²⁾ Together, these studies lead to the conclusion that *Runx2* is essential for normal crown formation. However, to date, it remains unknown whether and how *Runx2* regulates tooth root development.

Previously,⁽⁸⁾ we have identified that GLI1+ cells are progenitor cells in mouse molar root development: they show classic mesenchymal stem cell (MSC) characteristics in vitro and support root formation in vivo. To test the functional significance of *Runx2* in the regulation of tooth root development, we first analyzed RUNX2 expression during root development. Our data show that RUNX2 is expressed in a subpopulation of GLI1+ cells and that loss of *Runx2* in these GLI1+ cells results in root developmental defects. Furthermore, we identified several *Runx2* downstream target genes, shedding light on the molecular regulatory mechanism that controls tooth root development. Notably, we found that *Runx2* is required for WNT inhibitor *NOTUM* expression and regulates canonical WNT signaling to activate the odontoblastic lineage commitment of root progenitor cells during root development. This discovery highlights the specific signaling mechanism by which *Runx2* may exert its regulatory role during tooth root development.

Materials and Methods

Animal information

Mice used in this study included *Gli1-Cre^{ERT2}* knockin (JAX#007913; The Jackson Laboratory, Bar Harbor, ME, USA),⁽¹³⁾ *tdTomato* conditional reporter (JAX#007905; The Jackson Laboratory),⁽¹⁴⁾ conditional *Runx2* floxed (a gift from Dr. Yukio Yoneda, Kanazawa, Japan),⁽¹⁵⁾ *Gli1-LacZ* knockin/knockout reporter (JAX#008211; The Jackson Laboratory),⁽¹⁶⁾ *Runx2-rtTA* (a gift from Dr. Fanxin Long, Washington University, St. Louis, MO, USA),⁽¹⁷⁾ *terO-Cre* (JAX#006234; The Jackson Laboratory),⁽¹⁸⁾ and *Dmp1-Cre*.⁽¹⁹⁾ Mice were housed in pathogen-free conditions in the animal facility of the University of Southern California (USC). Mice were used for analysis irrespective of sex. Ear tissue was collected and lysed in DirectPCR reagent (Viagen Biotech, Inc., Los Angeles, CA, USA; #102-T) with Proteinase K (Viagen; #501-PK) at 85°C for 1 hour, followed by PCR-based genotyping. All the animal studies followed protocols approved by the Department of Animal Resources and the Institutional Animal Care and Use Committee of the University of Southern California.

Tamoxifen and doxycycline administration

Tamoxifen (Sigma-Aldrich, St. Louis, MO, USA; T5648) was dissolved in corn oil (Sigma-Aldrich; C8267) at 20 mg/mL and injected intraperitoneally once at postnatal day 3.5 (PN3.5) at a dose of 1.5 mg/10 g body weight. Doxycycline rodent diet (Envigo, Placentia, CA, USA; TD.08541) was administered every day from PN3.5 to PN7.5; meanwhile, doxycycline (Sigma-Aldrich; D9891) was dissolved in normal saline (NS) at 5 mg/mL

and injected intraperitoneally (i.p.) at PN3.5 and PN5.5 at a dose of 50 µg/g of body weight.

Histological analysis

Dissected mandibles were fixed in 4% paraformaldehyde for 24 hours and then decalcified in 10% EDTA (pH 7.4) for 1 to 4 weeks, depending on the age of the mice. For paraffin sectioning, decalcified samples were dehydrated in a Spin Tissue Processor (Thermo Fisher Scientific, Waltham, MA, USA), then embedded in paraffin and sectioned at 5 µm using a microtome (Leica Biosystems Inc., Buffalo Grove, IL, USA; RM2255). Hematoxylin and eosin (H&E) staining was performed using standard procedures. For frozen sectioning, decalcified samples were dehydrated in 15% sucrose/PBS solution followed by 30% sucrose/PBS solution, then embedded in 22-oxa-1,25-dihydroxyvitamin D₃ (OCT) compound (Tissue-Tek; Sakura Finetek USA, Inc., Torrance, CA, USA) and cryosectioned at 8 µm using a cryostat (Leica Biosystems Inc.; CM3050S). All the images were captured by an All-in-one Fluorescence Microscope (Keyence, Osaka, Japan; BZ-X710).

Immunostaining

Frozen sections were washed in PBS solution plus Tween-20 (PBST), blocked with TNB Blocking Buffer (PerkinElmer, Waltham, MA, USA; FP1020) for 1 hour, and incubated with primary antibody at 4°C overnight. After washing in PBST, sections were incubated with Alexa-conjugated secondary antibody for 1 hour at room temperature; 4,6-diamidino-2-phenylindole (DAPI) (Abcam, Cambridge, MA, USA; ab104139) was used for nuclear staining.

Antibodies used in our study were as follows: RUNX2 (Cell Signaling Technology, Beverly, MA, USA; 12556S, 1:200), β-Galactosidase (Abcam; ab9361, 1:500), Ki67 (Abcam; ab15580, 1:500), Goat anti-Rabbit IgG Alexa Fluor 488/568 (Invitrogen, Carlsbad, CA, USA; A11034, A11011, 1:200), and Goat anti-chicken IgY Alexa Fluor 568 (Invitrogen; A11041, 1:200).

RNAscope in situ hybridization

RNAscope 2.5 HD Reagent Kit-RED (Advanced Cell Diagnostics, Newark, CA, USA; 322350) and RNAscope Multiplex Fluorescent v2 (Advanced Cell Diagnostics; 323110) were used in our study to detect gene expression in situ on frozen sections, according to the manufacturer's instructions. All the probes were purchased from Advanced Cell Diagnostics, including *Dspp* (448301), *Gli1* (311001), *Pcp4* (402311), *Sfrp2* (400381), *NOTUM* (428981), *Axin2* (400331), *Wnt3a* (405041), and *Wnt4* (401101).

Micro-CT analysis

Fixed samples were scanned using a micro-CT (µCT) SCANCO µCT50 scanner (SCANCO Medical AG, Brüttisellen, Switzerland; V1.28) at the University of Southern California Molecular Imaging Center. The µCT images were captured at a resolution of 10 µm under an X-ray source of 90 kVp and 78 µA. Three-dimensional reconstruction was done using AVIZO 9.5 software (Thermo Fisher Scientific).

Quantitative RT-PCR

Mandibular first molars of PN7.5 or PN21.5 mice were carefully dissected on ice. Four mice were used for each group. The apical half of each molar was used for RNA extraction using RNeasy Plus Micro Kit (QIAGEN, Valencia, CA, USA; 74034). Quantitative RT-

PCR analysis was performed using iScript cDNA Synthesis kit (Bio-Rad Laboratories, Hercules, CA, USA), SsoFast EvaGreen Supermix (Bio-Rad Laboratories), and Bio-Rad CFX96 Real-Time Systems. Data analysis was following the $2^{-\Delta\Delta CT}$ method.⁽²⁰⁾ The primer sequences were obtained from PrimerBank (<https://pga.mgh.harvard.edu/primerbank/>) and are listed in Supplemental Table 1.⁽²¹⁾

Chromatin immunoprecipitation assay

Chromatin immunoprecipitation (ChIP) assay was performed using the apical halves of mandibular first molars of control PN7.5 mice, and tissues from approximately 20 mice were combined to comprise one sample. Chromatrap ChIP kit (Porvair Sciences, Norfolk, UK; 500191) was used in our experiment. After immunoprecipitation with anti-RUNX2 antibody (Cell Signaling; 12556S), or rabbit IgG (Chromatrap, Porvair Sciences), real-time qPCR was performed using the primers in Supplemental Table 1.

Bulk RNA sequencing analysis

Gli1-Cre^{ERT2};Runx2^{fl/fl} and *Runx2^{fl/fl}* littermate control mice received injection of tamoxifen at PN3.5 and were euthanized 4 days later. The apical halves of the mandibular first molars were dissected for RNA extraction. Each sample contained tissues from four mice. cDNA library preparation and sequencing were carried out by the Technology Center for Genomics & Bioinformatics at the University of California, Los Angeles (UCLA). A total of 200 million pair-end reads were obtained on NovaSeq 6000 S2 (Illumina, San Diego, CA, USA) for four pairs of samples. The raw data was analyzed using Partek[®] Flow[®] software (Partek Incorporated, St. Louis, MO, USA). Briefly, raw reads were trimmed, aligned by STAR (2.6.1d; <https://github.com/alexdobin/STAR/releases>) with the mm10 genome, and normalized using the fragments per kilobase of transcript per million mapped reads (FPKM) method. Differential analysis was performed using the gene set analysis (GSA) method. Value of $p < 0.05$ and fold change < -1.8 or > 1.8 across groups were considered significant.

Single-cell RNA sequencing analysis isolation of cells and sequencing

Gli1-Cre^{ERT2};Runx2^{fl/fl} and *Runx2^{fl/fl}* littermate control mice were injected with tamoxifen at PN3.5 and euthanized 4 days later. Whole mandibular first molars were collected in PBS on ice, with each sample containing eight molars total from four mice. Then the molars were cut into small pieces and transferred into digestion solution (2 mg/mL Collagenase I + 2 mg/mL Dispase, dissolved in Hank's balanced salt solution [HBSS]). Samples were incubated at 37°C with rotation in a Hybaid Oven (Thermo Scientific, Waltham, MA, USA) for 25 min, with occasional pipetting. Then the samples were passed through a Flowmi[®] cell strainer (porosity 40 μ m) (SP Scienceware, Warminster, PA, USA) to obtain a single-cell suspension. The Chromium Single Cell 3' Reagent Kits v3 (10X Genomics, San Francisco, CA, USA) was used for gel bead-in emulsions (GEM) generation and library construction, according to the protocols provided by the manufacturer. The cDNA sequencing was conducted by the Technology Center for Genomics & Bioinformatics at UCLA. Quality control, mapping, and count table assembly of the library were performed using the CellRanger pipeline version 3.1.0 (10X Genomics).

Integration analysis of control and mutant samples

Raw read counts from the control and *Gli1-Cre^{ERT2};Runx2^{fl/fl}* sample were analyzed using the Seurat v3 R package (R Foundation for Statistical Computing, Vienna, Austria; <https://www.r-project.org/>).^(22,23) Data were first filtered and normalized, then the FindVariableGenes function was used to select variable genes. The FindIntegrationAnchors function was used to identify "anchors" across the two datasets, which were then used to integrate the two datasets with the IntegrateData function. Scaledata, principal component analysis (PCA) and uniform manifold approximation and projection (UMAP) visualization were then performed for downstream analysis and visualization.

Assay for transposase-accessible chromatin sequencing analysis

The transposase-accessible chromatin sequencing (ATAC-seq) analysis was performed following standard protocols.⁽²⁴⁾ Briefly, the apical halves of eight mandibular first molars of PN7.5 *Runx2^{fl/fl}* control mice were collected in PBS on ice. Then the tissues were treated with the same method described in the Single-cell RNA sequencing (scRNA-seq) section to obtain a single-cell suspension. A total of 50,000 cells were lysed, and followed by transposition reaction and purification, and PCR amplification. The library construction and sequencing were performed by the Molecular Genomics Core at the University of Southern California, Los Angeles (USC). The raw data was analyzed using Partek[®] Flow[®] software. Briefly, raw reads were aligned using Bowtie2 (<http://bowtie-bio.sourceforge.net/bowtie2/index.shtml>) with the mm10 genome; Model-based Analysis of ChIP-Seq (MACS2) was used for detecting genomic enrichment regions; RUNX2 binding motifs were analyzed using Hypergeometric Optimization of Motif Enrichment (HOMER; <http://homer.ucsd.edu/homer/>).⁽²⁵⁾ Output files were uploaded to the UCSC genome browser (<https://genome.ucsc.edu/>) for visualization.

Cell culture and odontoblastic differentiation

Dental pulp tissue from the mandibular first molars of 10 PN7.5 mice was obtained, minced into small pieces, and seeded on a 6-cm cell-culture dish (Corning, Corning, NY, USA) with α -MEM + 10% FBS (Gibco, Grand Island, NY, USA) at 37°C in a 5% CO₂ incubator. When the primary cells reached 80% confluent, the cells were passed for odontoblastic differentiation. The odontoblastic differentiation medium contained 1% FBS, 5mM β -glycerophosphate (Sigma-Aldrich; G9422), 50 μ g/mL ascorbic acid (Sigma-Aldrich; A4403), and 1×10^{-7} M dexamethasone (Sigma-Aldrich; D4902).⁽²⁶⁾

Kidney capsule transplantation

Gli1-Cre^{ERT2};Runx2^{fl/fl} and *Runx2^{fl/fl}* littermate control mice were injected with tamoxifen at PN3.5 and euthanized 2 days later. Whole mandibular first molars were carefully dissected and placed in PBS on ice. Host mice were anesthetized using isoflurane, then fur on the back was shaved and the kidney on the left side was exposed through a skin incision. The kidney capsule was opened using fine-tip forceps. Two explants were transplanted under the kidney capsule of one host. Three weeks later, the explants were harvested for histological analysis. For the rescue experiment, Affi-Gel blue agarose beads (Bio-Rad Laboratories; 1537301) were washed in PBS and then incubated in recombinant mouse NOTUM protein (100 μ g/mL; R&D Systems, Minneapolis, MN, USA; 9150-NO)

or bovine serum albumin (BSA) (100 µg/mL) for 1 hour at 37°C before transplantation. NOTUM beads or BSA beads were then applied to the explants from *Gli1-Cre^{ERT2};Runx2^{fl/fl}* mice and transplanted under the kidney capsule.

Statistical analysis

GraphPad Prism 8 (GraphPad Software, Inc., La Jolla, CA, USA) and Microsoft Office 2016 (Microsoft Corp., Redmond, WA, USA) were used for statistical analysis. Results are represented as box-plots showing each data point, the median and the interquartile range. Significance was assessed by independent two-tailed Student's *t* tests; *p* < .05 was considered statistically significant. *n* ≥ 3 for sample size; all experiments were repeated in triplicate or more to confirm the results unless otherwise stated.

Results

RUNX2 expression overlaps with a subpopulation of GLI1+ cells during root development

RUNX2 is expressed throughout tooth crown development, which occurs mainly at embryonic stages in mice.⁽²⁷⁾ Shortly after tooth development initiates, RUNX2 expression is already detectable in the odontogenic mesenchyme, and remains strong during the bud and cap stages, but is downregulated at the bell and postnatal stages.⁽¹¹⁾ To determine whether *Runx2* is associated with root development, we examined the expression pattern of RUNX2 at different stages of root development and compared the pattern to that of GLI1+ cells and their progeny. At PN3.5, prior to root formation, RUNX2 is expressed in the apical dental papilla, dental follicle, and surrounding bones, and its expression overlaps with a subset of the GLI1+ cells in the apical region of the dental mesenchyme (Fig. 1A–D). We also performed lineage tracing of GLI1+ cells to label their progeny from PN3.5. Four days later, upon the initiation of root formation, GLI1+ cells were present in the root-forming apical mesenchyme and dental epithelium, whereas RUNX2 expression colocalized with them in a more restricted area around Hertwig's epithelial root sheath (HERS), an epithelial structure that guides root formation, as well as in the preodontoblast region (Fig. 1E–H). At PN21.5, when root development is complete, progeny of these GLI1+ cells contributed to the entire root structure, including odontoblasts, pulp cells, periodontal ligament, alveolar bone, and the remaining dental epithelium; they colocalized with RUNX2 in the periodontal ligament, alveolar bone, and some odontoblasts (Fig. 1I–L, Supplemental Fig. 2A–C). These results suggest RUNX2 expression overlaps with a subpopulation of GLI1+ cells during root development, and RUNX2 may be essential for GLI1+ progenitor cells to differentiate into odontoblasts and other root structures.

To test whether RUNX2+ cells are progenitor cells, we analyzed their contribution to the dental mesenchyme during tooth root development. RUNX2+ cells in *Runx2-rtTA;TetO-Cre;TdTomato^{fl/+}* mice were labeled by doxycycline administration from PN3.5 to PN7.5. After labeling at PN7.5, we located RUNX2+ cells (tdTomato+) in the most apical region of the dental papilla, in the dental follicle and in odontoblasts (Supplemental Fig. 1A,B). Eighteen days later, only a few odontoblasts and pulp cells were labeled (Supplemental Fig. 1C,D), indicating that RUNX2+ cells do not contribute to root growth, and therefore are not root progenitor cells. As a

technical matter, we note that *Runx2-rtTA* is a BAC transgenic line with the cDNA for rtTA2^S-M2 replacing the first exon of the *Runx2* gene. Previously published work suggests that *Runx2-rtTA* targets osteoblast-lineage cells.⁽¹⁷⁾ RUNX2 has two major N-terminal isoforms: RUNX2-I is encoded by exons 2 to 8, whereas RUNX2-II is encoded by exons 1 to 8, which means *Runx2-rtTA* may only target the RUNX2-II-expressing cells.

Loss of *Runx2* results in tooth root development defects

Although RUNX2+ cells have limited contribution to the root growth, they are located in the region of GLI1+ progenitor cells. To test the significance of *Runx2*'s function for tooth root development, we generated *Gli1-Cre^{ERT2};Runx2^{fl/fl}* mice and administered tamoxifen at PN3.5 to specifically delete *Runx2* in GLI1+ root progenitor cells and their progeny before the initiation of root formation. We confirmed that *Runx2* was efficiently deleted by tamoxifen induction, with no RUNX2 expression detectable in the dental mesenchyme of *Gli1-Cre^{ERT2};Runx2^{fl/fl}* mice (Supplemental Fig. 2A–F). Ablation of *Runx2* resulted in severe root development defects (Fig. 2A–J). At PN21.5, the molar roots in control mice were well developed and had erupted, and the odontoblasts, pulp cells, periodontal ligament, and alveolar bone were properly formed (Fig. 2A,B,E–G). In contrast, the roots in *Gli1-Cre^{ERT2};Runx2^{fl/fl}* mice were much shorter and the teeth had not yet erupted, although the crowns appeared to be normal (Fig. 2C,D,H, and Supplemental Fig. 2G). In addition, the root dentin was much thinner, and the root odontoblasts lost their columnar structure, although the nuclei were not polarized (Fig. 2H–J). Consistent with impaired odontoblast differentiation, the expression of dentin sialophosphoprotein (*Dspp*), a marker of odontoblast differentiation, was absent in the root region (Fig. 2K,N, and Supplemental Fig. 2H), suggesting *Runx2* is required for the odontoblastic lineage commitment of GLI1+ root progenitor cells. The formation of the periodontal ligament, cementoblasts, and alveolar bone was also deficient in *Gli1-Cre^{ERT2};Runx2^{fl/fl}* mice (Fig. 2H–J). Moreover, we found that there were more proliferating cells in the apical dental mesenchyme around HERS (Fig. 2L,M,O,P, and Supplemental Fig. 2I), probably due to these cells failing to differentiate in *Gli1-Cre^{ERT2};Runx2^{fl/fl}* mice. This was further confirmed by lineage tracing of GLI1+ cells after deletion of *Runx2* in *Gli1-Cre^{ERT2};Runx2^{fl/fl};tdTomato^{fl/+}* mice. The progeny of GLI1+ cells remained in the apical area, failing to contribute to root elongation and the formation of periodontium and alveolar bone as observed in control mice (Supplemental Fig. 2A–F).

The *Gli1-Cre^{ERT2};Runx2^{fl/fl}* mice also developed a severe CCD-like phenotype, characterized by smaller body size and impaired skeletal development, including delayed cranial suture closure, hypoplastic clavicles, and micrognathia (Supplemental Fig. 3A–I). Heterozygous mutation of *RUNX2* in humans and mice can cause CCD,^(10,28) but we failed to detect any bone formation defects (data not shown) or root formation defects in *Gli1-Cre^{ERT2};Runx2^{fl/+}* mice (Supplemental Fig. 4D–F). These results may indicate that *Runx2* also plays an important role at earlier stages in GLI1+ cells, and/or that it is important in GLI1– cells as well as in GLI1+ cells. Because *Runx2* is also expressed in mature odontoblasts, to investigate whether loss of *Runx2* in these cells has an effect on root development, we generated *Dmp1-Cre;Runx2^{fl/fl}* mice but did not identify any obvious defect in dentinogenesis (Supplemental Fig. 4G–I), suggesting that loss of *Runx2* in mature odontoblasts does not affect odontoblast

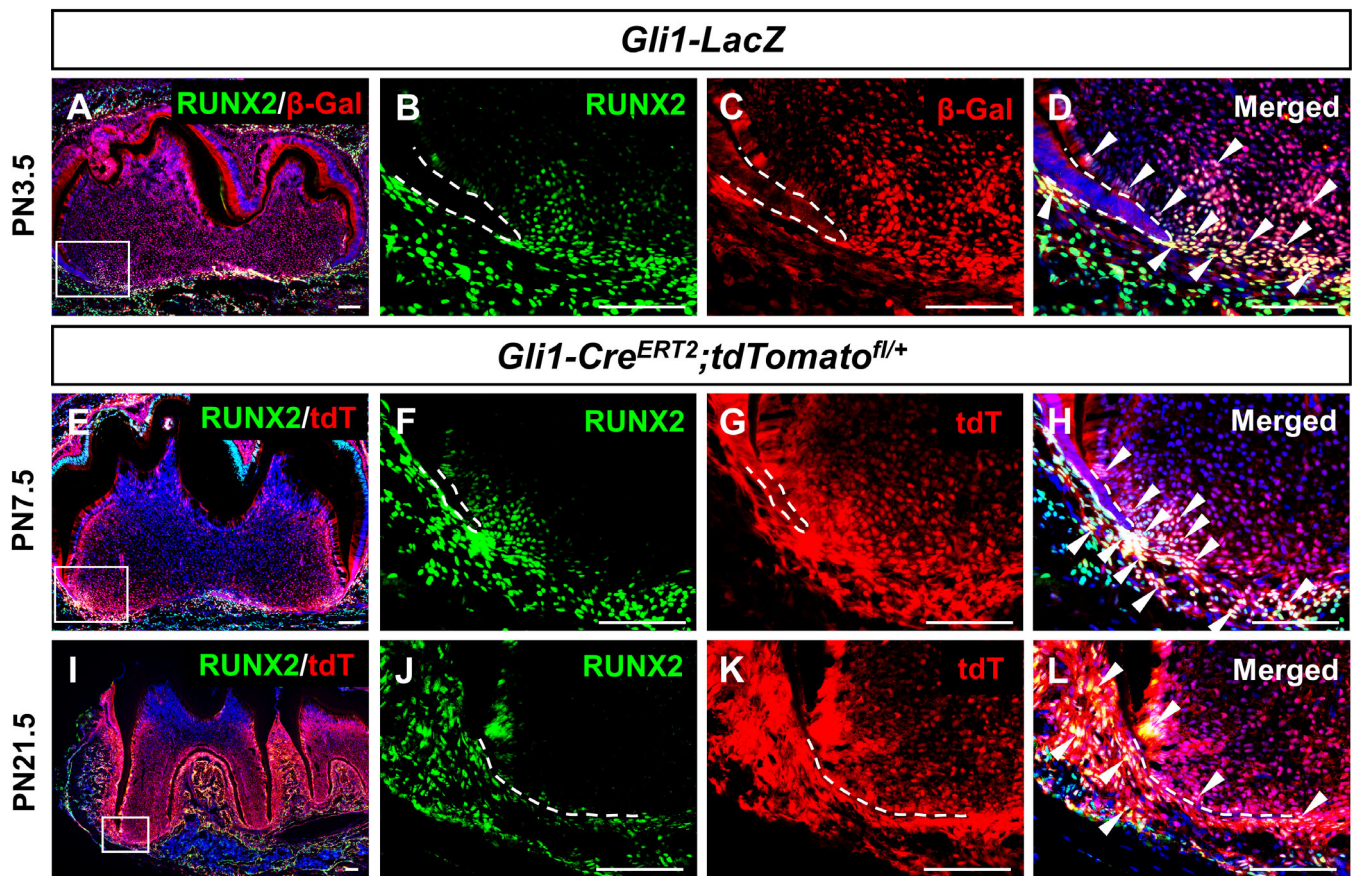


Fig 1. Colocalization of RUNX2 and GLI1+ MSCs and their progeny in developing roots. (A–D) RUNX2 (green) and GLI1 (stained by β -gal in red) co-immunofluorescence of sagittal sections of mandibular molars from PN3.5 heterozygous *Gli1-LacZ* mice. (E–L) RUNX2 immunofluorescence (green) and visualization of tdT (red) of sagittal sections of mandibular molars from *Gli1-Cre^{ERT2};tdTomato^{fl/+}* mice at PN7.5 (E–H) and PN21.5 (I–L) after induction at PN3.5. The progeny of the GLI1+ lineage are presented in red. Boxes in A, E, and I are enlarged in B–D, F–H, and J–L, respectively. White dashed lines outline HERS; arrows indicate colocalization. Scale bars = 100 μ m. β -gal = β -galactosidase; tdT = tdTomato.

differentiation or root elongation. Taken together, our studies suggest that *Runx2* is indispensable for the differentiation of GLI1+ root progenitor cells to support root formation.

Identification of *Runx2* downstream target genes during root development

To identify downstream targets of *Runx2* that may regulate GLI1 + MSC differentiation, we collected the apical halves of molars at PN7.5—4 days after Tamoxifen induction from both control and *Gli1-Cre^{ERT2};Runx2^{fl/fl}* mice for bulk RNA sequencing. In total, 427 genes were differentially expressed between these two groups, among them 219 upregulated and 208 downregulated in *Gli1-Cre^{ERT2};Runx2^{fl/fl}* mice, and the heat map displays a distinct separation between the groups (Fig. 3A).

To map the differentially expressed genes back to their anatomic location at single-cell resolution, we conducted scRNA-seq of whole PN7.5 molars from control and *Gli1-Cre^{ERT2};Runx2^{fl/fl}* mice to distinguish the expression patterns of these differentially expressed genes. A total of 4394 cells from control mice and 4764 cells from *Gli1-Cre^{ERT2};Runx2^{fl/fl}* mice were sequenced, and a median of 1615 genes were read out per cell, suggesting the two samples were quite comparable. We

performed integration analysis of the control and *Gli1-Cre^{ERT2};Runx2^{fl/fl}* sequencing data using Seurat v3. The cells were divided into 19 clusters based on their distinct gene expression profiles (Fig. 3B). Cells color-coded by sample suggested there was not a major shift in the cell distribution between control and *Gli1-Cre^{ERT2};Runx2^{fl/fl}* mice (Supplemental Fig. 5B). Cells in clusters 0, 1, 3, and 4 were identified as dental papilla cells by marker genes *Slc20a2* and *Msx2* (Fig. 3B),^(29,30) whereas cluster 15 represented odontoblasts marked by *Dspp* (Supplemental Fig. 5C). Cluster 2 was identified as dental follicle cells by marker genes *Bmp3* and *Spon1* (Fig. 3B).⁽³¹⁾ The other clusters represented dental epithelium (clusters 9, 11, 12, 13, 14), endothelial cells (cluster 8), immune cells (clusters 5, 6, 7, 10, and 17), and glia (clusters 16, 18) (Supplemental Fig. 5C).

The most enriched genes of each cluster within the dental papilla were used to map the clusters to their anatomic locations. Two marker genes of cluster 1, *Dio3* and *Itga4*, were found to be expressed in the apical dental mesenchyme (Fig. 3C,D), where root formation initiates, suggesting cells in cluster 1 are associated with root formation. We integrated the differentially expressed genes identified in the bulk RNA-seq analysis with their expression profiles revealed by scRNA-seq to verify specific downstream targets of *Runx2*. We identified a number of genes that were enriched in

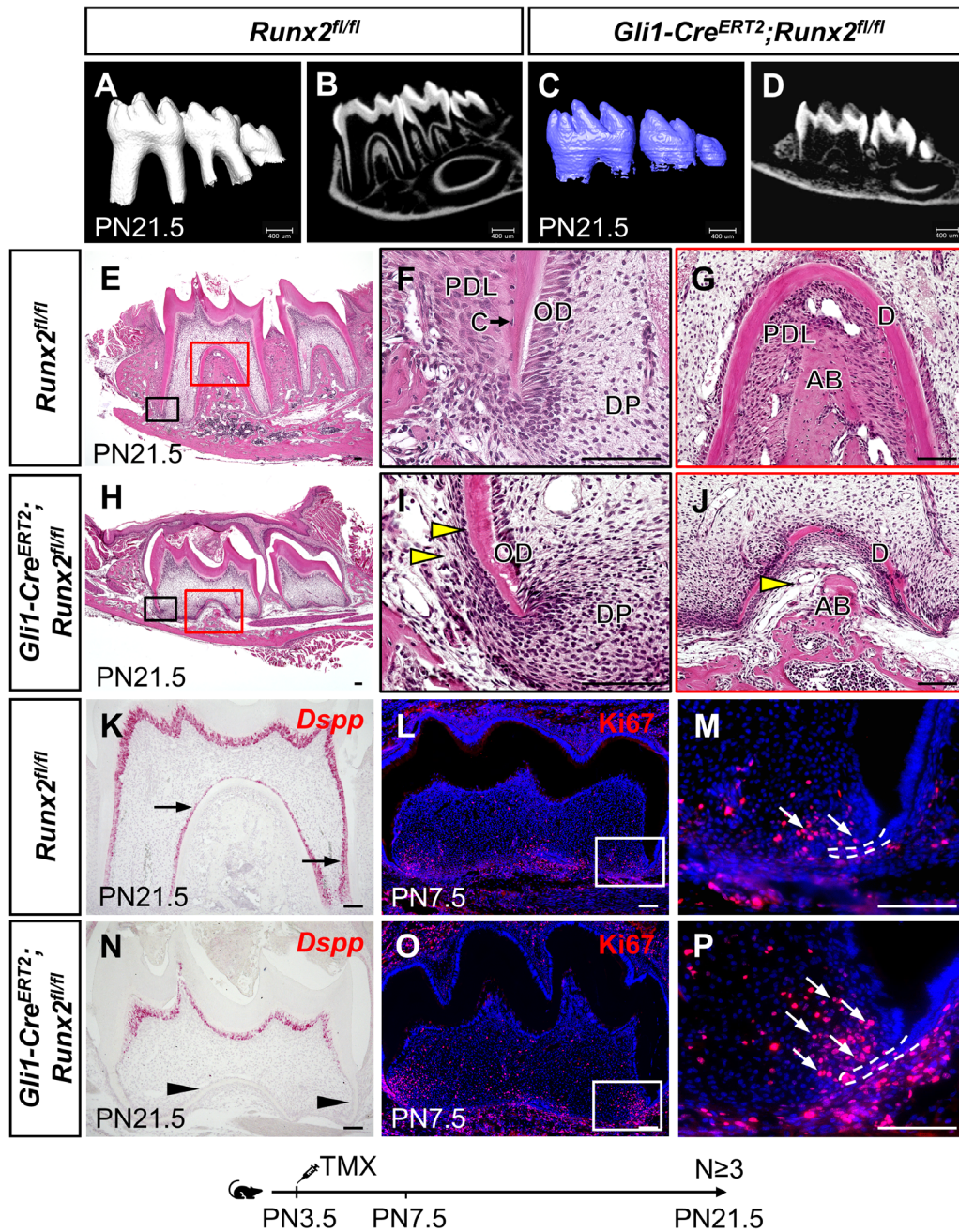


Fig 2. Loss of *Runx2* in GLI1+ MSCs results in root development defects. (A–D) μ CT images of *Runx2*^{fl/fl} control (A,B) and *Gli1-Cre*^{ERT2};*Runx2*^{fl/fl} (C,D) mandibular molars at PN21.5. (E–J) H&E staining of *Runx2*^{fl/fl} control (E–G) and *Gli1-Cre*^{ERT2};*Runx2*^{fl/fl} (H–J) mandibular molars at PN21.5. Boxed areas in E and H are shown magnified in F–G and I–J, respectively. Yellow arrowheads indicate the absence of cementoblasts and periodontal ligament. (K–P) *Dspp* in situ hybridization (red) at PN21.5 (K,N), and Ki67 immunofluorescence (red) indicating proliferating cells at PN7.5 (L,M,O,P) in sagittal sections of mandibular molars in *Runx2*^{fl/fl} control and *Gli1-Cre*^{ERT2};*Runx2*^{fl/fl} mice. Arrows in K, M, and P indicate positive signals; arrowheads in N indicate absence of signal. Boxes in L and O are enlarged in M and P, respectively. Dashed white lines outline HERS. Scale bars in A–D = 400 μ m; scale bars in all others = 100 μ m. AB = alveolar bone; C = cementoblast; D = dentin; DP = dental pulp; OD = odontoblast; PDL = periodontal ligament.

cluster 1 that had significant differences in signal quantity and intensity, namely *Gli1*, *Pcp4*, *NOTUM*, and *Sfrp2* (Fig. 3E, Supplemental Fig. 6A–D). The differences in the expression levels of these candidate genes were validated by RNAscope in situ hybridization (Fig. 4E–T) and qPCR (Supplemental Fig. 6E–H), and their expression was assessed for overlap with RUNX2 in developing molars (Fig. 4A–D). *Gli1* and *Pcp4* were expressed in the apical region of

the dental mesenchyme in control mice, especially close to HERS, whereas their expression was sharply decreased in *Gli1-Cre*^{ERT2};*Runx2*^{fl/fl} mice (Fig. 4E–L). *NOTUM* was expressed solely in the progenitors of odontoblast next to HERS in control mice, whereas its expression almost vanished in *Gli1-Cre*^{ERT2};*Runx2*^{fl/fl} mice (Fig. 4M–P). *Sfrp2* expression was found predominantly in the dental follicle in control mice, and its expression was also significantly

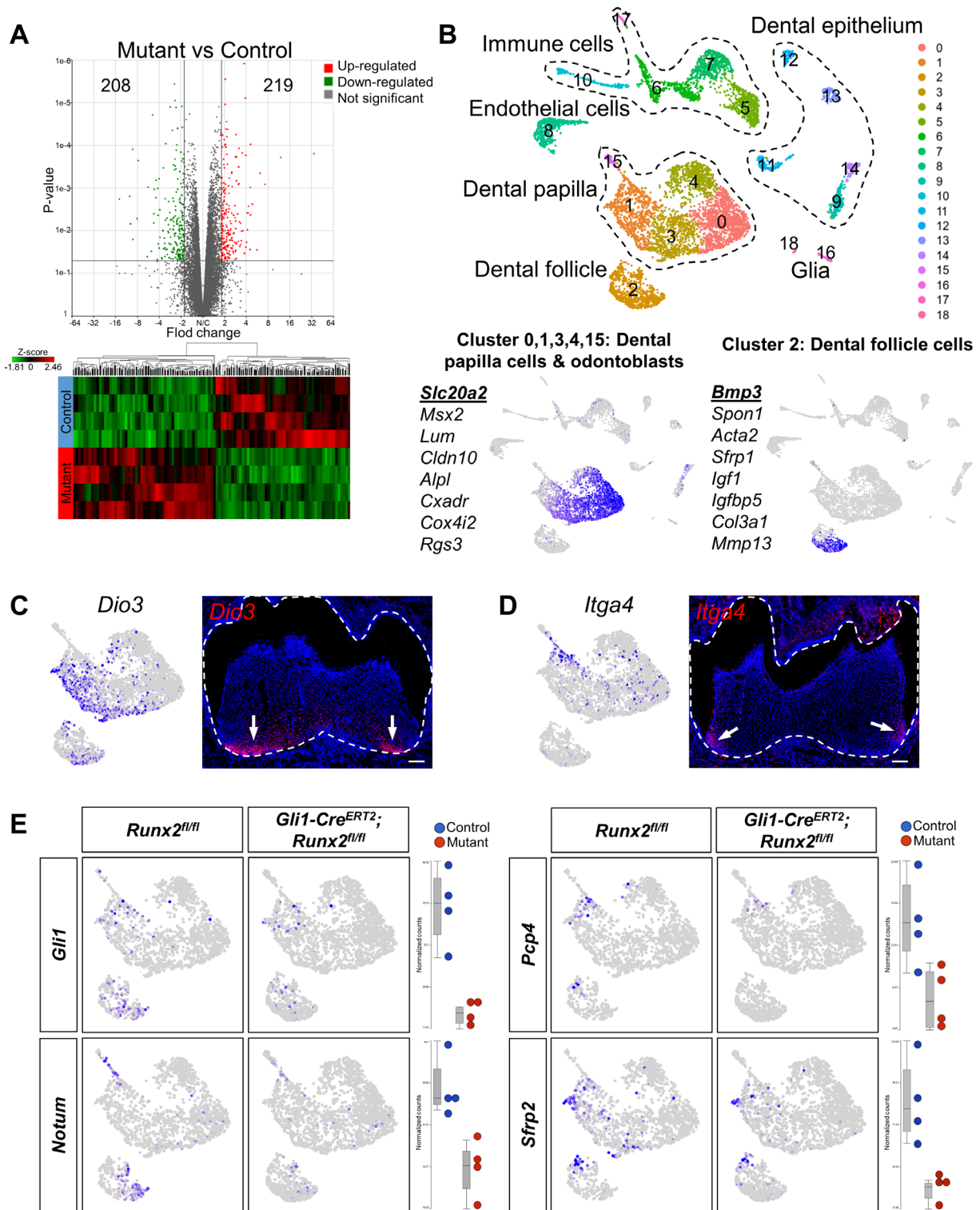


Fig 3. Integrated analysis of bulk RNA-seq and scRNA-seq reveals specific downstream targets of *Runx2*. (A) Bulk RNA-seq revealed that 219 genes were upregulated and 208 genes were downregulated with >1.8-fold change ($p < .05$) upon *Runx2* deletion, represented here by volcano plot and heat map. (B) UMAP plots showed 19 clusters within PN7.5 molars after integration of the *Runx2^{fl/fl}* control and *Gli1-Cre^{ERT2};*Runx2^{fl/fl}** scRNA sequencing data with Seurat v3. Different clusters represent different cell types in the mouse molar, defined by expression of known marker genes. Dashed lines outline clusters representing the same cell type. Clusters 0, 1, 3, 4, and 15: dental papilla cells and odontoblasts. Cluster 2: dental follicle cells. The feature plot of the first gene in the list is shown. (C,D) Cluster 1 maps to the apical region of dental mesenchyme by two marker genes, *Dio3* (C) and *Itga4* (D). Dashed white lines outline tooth, arrows indicate positive signals. Scale bars = 100 μ m. (E) Feature plots and box plots of four differentially expressed genes mapping to cluster 1. They were identified as potential downstream targets of *Runx2*. The differences in expression levels were consistent between feature plots of scRNA-seq and box plots of bulk RNA-seq.

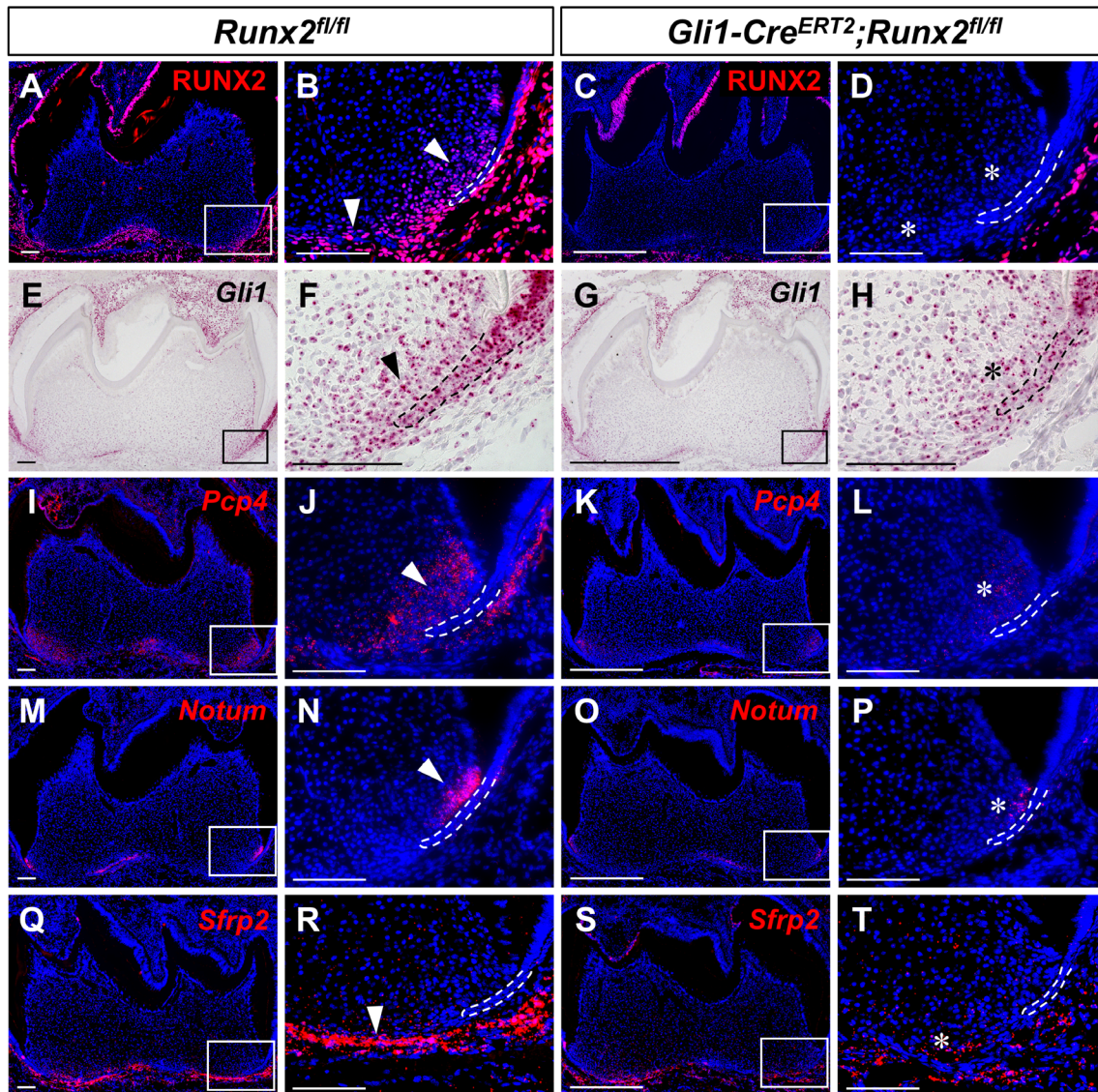


Fig 4. In vivo validation of putative downstream targets upon deletion of *Runx2* in the dental mesenchyme. RUNX2 immunofluorescence (A–D) and RNA-scope in situ hybridization (red) of *Gli1* (E–H), *Pcp4* (I–L), *NOTUM* (M–P), and *Sfrp2* (Q–T) of sagittal sections of mandibular molars from PN7.5 *Runx2^{fl/fl}* control and *Gli1-Cre^{ERT2};Runx2^{fl/fl}* mice. The boxed area is enlarged on the right. Dashed lines outline HERS. Arrowhead indicates positive signals; asterisks indicate altered staining in targeted region of mutant samples. $n = 3$ sections were examined from multiple littermate mice per group. Scale bars = 100 μm .

decreased in *Gli1-Cre^{ERT2};Runx2^{fl/fl}* mice (Fig. 4Q–T); therefore, it was most likely to be associated with periodontal tissue development. These findings suggest that integration of data on differentially expressed genes from complementary bulk and scRNA-seq analyses can help to verify downstream targets efficiently. It was interesting to find that *NOTUM* expression concentrated in the preodontoblast region, which indicates that *NOTUM* may play an important role in the odontoblastic lineage commitment of the GLI1+ progenitor cells.

Runx2 determines odontoblastic differentiation of GLI1+ MSCs via inhibition of WNT signaling through a WNT inhibitor, *NOTUM*

NOTUM is a recently identified WNT antagonist that acts via inactivation of WNT ligands.^(32,33) Because *NOTUM* expression

was almost undetectable in the *Runx2* mutant molars (Fig. 4M–P), we further examined WNT signaling activity using *Axin2* as a readout. We found that *Axin2* expression was increased in the apical region of the mesenchyme around HERS, especially in the preodontoblast region of *Gli1-Cre^{ERT2};Runx2^{fl/fl}* mice, where *NOTUM* signals vanished (Supplemental Fig. 7A–D, I), suggesting that loss of *NOTUM* resulted in upregulation of WNT signaling in the apical dental mesenchyme. We also found that WNT ligands *Wnt3a* and *Wnt4* were expressed in the nearby dental epithelial structure of HERS (Supplemental Fig. 7E–H). Considering these findings, we hypothesized that the WNT inhibitor *NOTUM* protein inactivates WNT ligands *WNT3a* and *WNT4*, which are secreted by dental epithelium, thereby mediating the level of WNT activity in the dental mesenchyme that is essential for the odontoblastic lineage commitment of GLI1+ MSCs.

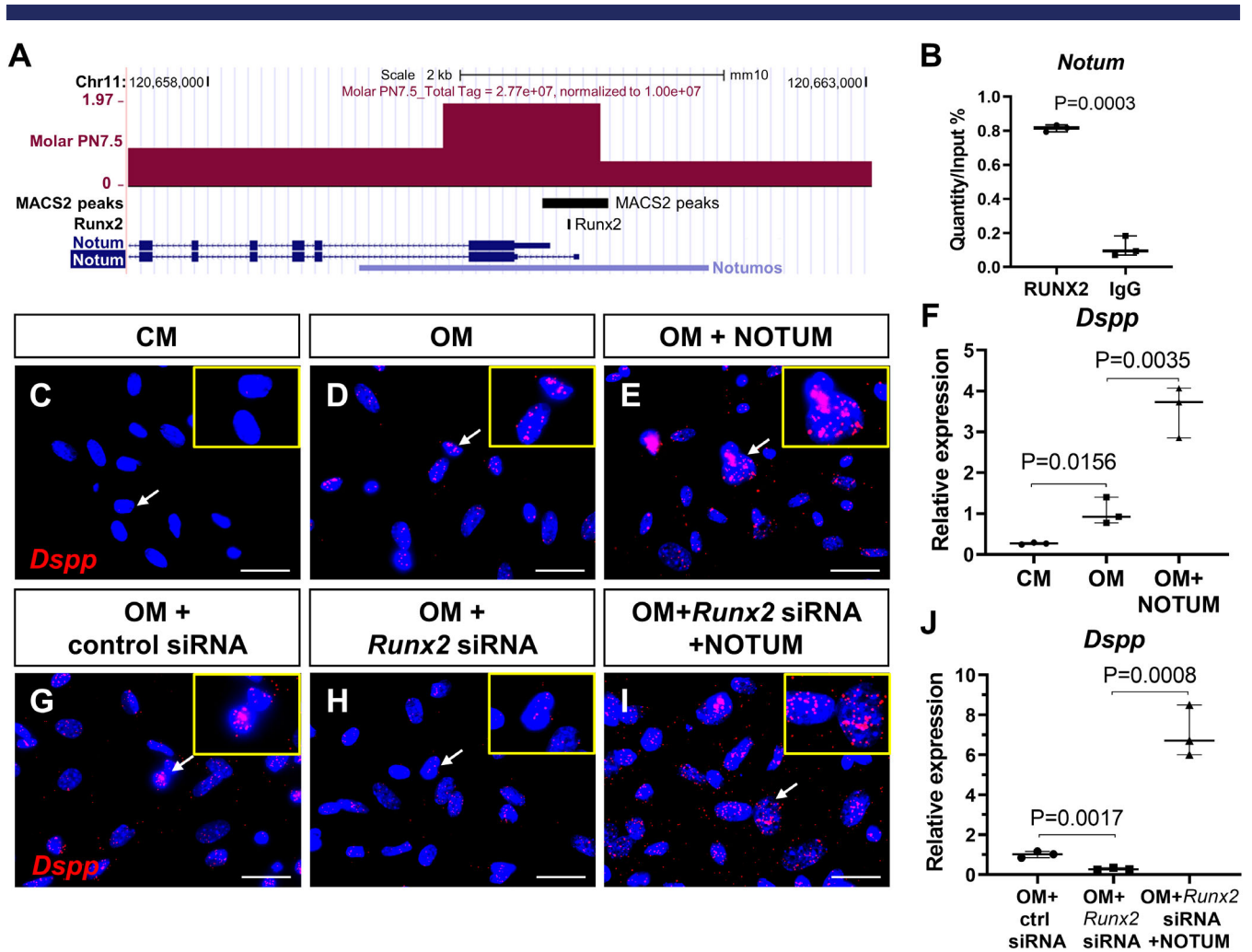


Fig 5. *NOTUM* is a direct target of *RUNX2* and activates the expression of odontoblast marker *Dspp* in vitro. (A) Genome browser snapshots representing the peak of ATAC-seq from PN7.5 control mouse molars colocalized with the *RUNX2* binding site at the promoter region of *NOTUM*. (B) ChIP analysis revealed the binding of endogenous *RUNX2* to the genomic loci of *NOTUM*. DNA before immunoprecipitation (input) and after immunoprecipitation with an anti-*RUNX2* or rabbit IgG was amplified by qPCR using primers that amplify the regions containing *RUNX2*-binding motifs in the *NOTUM* promoter. The value of input was defined as 1, and relative levels are shown. (C–J) RNAse in situ hybridization (red) and qPCR of *Dspp* in cultured dental pulp cells treated with CM, OM, and OM + *NOTUM* protein (C–F), as well as OM + control siRNA, OM + *Runx2* siRNA, and OM + *Runx2* siRNA + *NOTUM* protein (G–J), insets in C–E and G–I are enlarged images of the cells pointed to by arrows in the same image. Scale bars = 25 μ m. CM = control growth media; OM = odontoblastic media.

To examine the interaction between *Runx2* and *NOTUM*, we collected the apical dental mesenchymal tissue from control mandibular first molars at PN7.5 for ATAC-seq. The chromosome view showed there was an open chromatin signal and a MACS2 peak at the promoter region of *NOTUM* (Fig. 5A) and promoter prediction identified a *RUNX2* binding site in the same region, suggesting that *NOTUM* was actively transcribed and that *RUNX2* may regulate its transcription. ChIP analysis revealed that endogenous *RUNX2* binds to the genomic loci of *NOTUM* (Fig. 5B). Our results therefore indicate that *RUNX2* directly regulates *NOTUM* expression to control root development.

Exogenous *NOTUM* partially rescues the root defects in *Gli1-Cre^{ERT2};Runx2^{fl/fl}* mice

Because *NOTUM* expression is centralized in the preodontoblast region and may guide odontoblastic differentiation, we sought

to determine whether *NOTUM* could rescue the odontoblast differentiation defects we observed in *Gli1-Cre^{ERT2};Runx2^{fl/fl}* mice. First we cultured the dental pulp cells from control mouse molars, then added *NOTUM* protein to the odontoblast differentiation medium. As expected, exogenous *NOTUM* significantly promoted odontoblast differentiation by activating the odontoblast-specific marker *Dspp* (Fig. 5C–F). Moreover, exogenous *NOTUM* could rescue the impaired odontoblast differentiation after *Runx2* siRNA-mediated knockdown in vitro (Fig. 5G–J, Supplemental Fig. 8).

We further tested whether ectopic *NOTUM* protein could rescue the root defects in *Gli1-Cre^{ERT2};Runx2^{fl/fl}* mice using kidney capsule transplantation. In control explants, the teeth developed two normal roots. The newly formed root dentin was thick and predentin was detectable, indicating that active dentinogenesis occurred, and the odontoblasts were polarized and columnar (Fig. 6A,D,G). In the *Gli1-Cre^{ERT2};Runx2^{fl/fl}* molar explants with

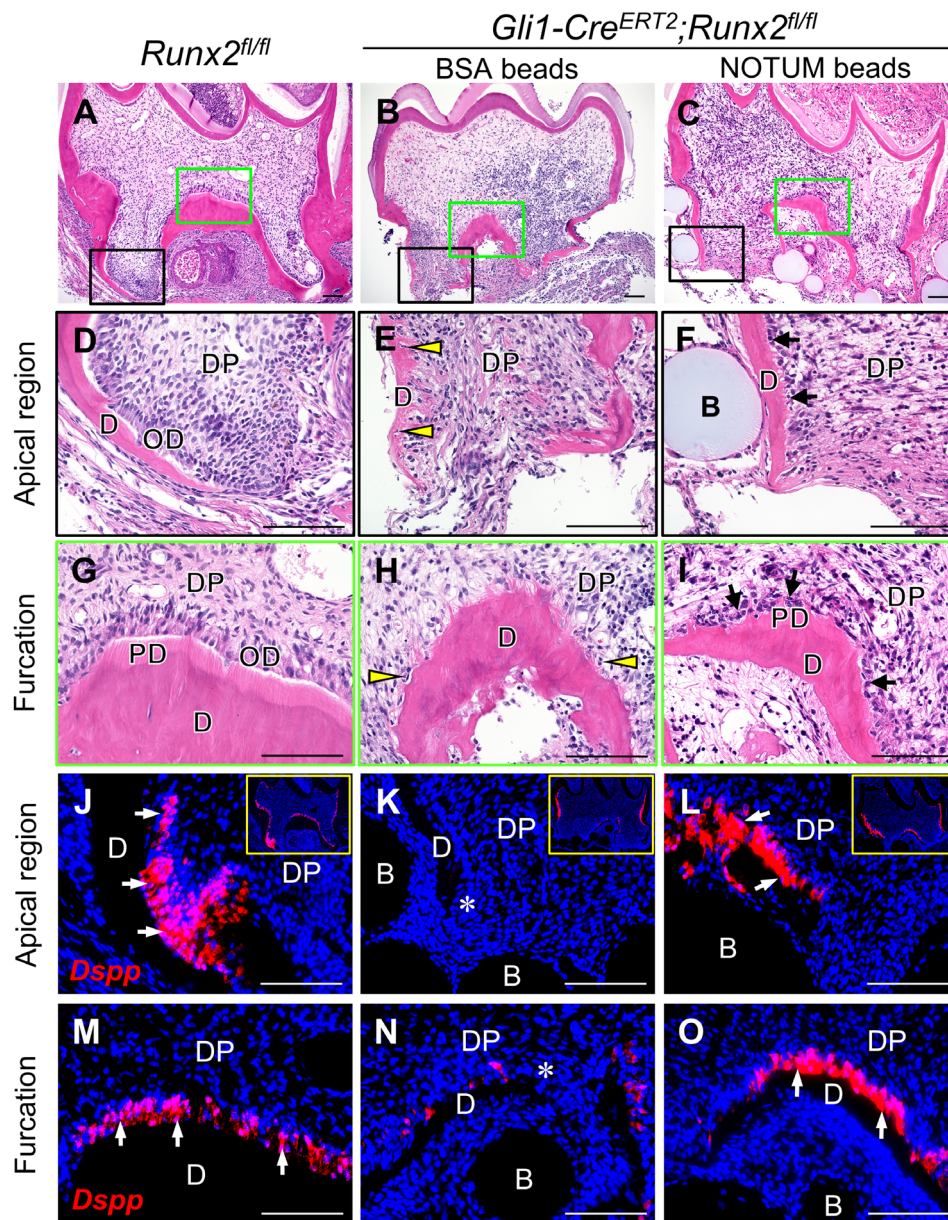


Fig 6. Ectopic NOTUM partially rescues the root defect in *Gli1-Cre^{ERT2};Runx2^{fl/fl}* mice. H&E staining (A–I) and RNAscope in situ hybridization of *Dspp* (J–O) of sagittal sections of tooth germs from *Runx2^{fl/fl}* control and *Gli1-Cre^{ERT2};Runx2^{fl/fl}* mice cultured for 3 weeks under kidney capsules with BSA or NOTUM beads. The control explants developed well; two roots with columnar odontoblasts, thick dentin, and predentin are identifiable (A,D,G). In *Gli1-Cre^{ERT2};Runx2^{fl/fl}* molars treated with BSA beads (B,E,H), the root dentin is irregular, and predentin is unseen, arrowheads indicate there are few odontoblast-like cells along with the dentin, some cells are embedded into the dentin. After treatment with NOTUM beads (C,F,I), the root dentin became more regular with detectable predentin, and many odontoblast-like cells accumulated at the surface of the dentin (indicated by black arrows). *Dspp* expression is strong in control samples (J,M), whereas in *Gli1-Cre^{ERT2};Runx2^{fl/fl}* molars treated with BSA beads (K,N), there are only a few positive signals. Following treatment with NOTUM beads, *Dspp* is detectable in the apical region (L) and furcation region (O). Insets in J, K, and L are lower magnification images of the same sample. White arrows indicate positive signal; asterisks indicate absence of signal. B = bead; D = dentin; PD = predentin; DP = dental pulp; OD = odontoblast. *n* = 4 samples were collected and analyzed for each group. Scale bars = 100 μ m.

BSA beads, the roots were shorter and irregular with thinner dentin, predentin was absent, and odontoblasts were undetectable along with the dentin (Fig. 6B,E,H). In contrast, after treatment with NOTUM beads, the root dentin of *Gli1-Cre^{ERT2};Runx2^{fl/fl}* molar explants became more regular, predentin was present, and odontoblast-like cells accumulated at the surface of the dentin, although they were not columnar in shape (Fig. 6C,F,

I). Furthermore, there was almost no expression of odontoblast marker *Dspp* in the roots of *Gli1-Cre^{ERT2};Runx2^{fl/fl}* molar explants with BSA beads (Fig. 6K,N), compared to the control group (Fig. 6J,M); in contrast, in the *Gli1-Cre^{ERT2};Runx2^{fl/fl}* molar explants with NOTUM beads, *Dspp* expression became detectable in the root apical region near the beads, as well as the furcation region (Fig. 6L,O), suggesting that there were

some differentiated odontoblasts. However, the root length was not restored after treatment with NOTUM beads (Supplemental Fig. 9). These results suggest that NOTUM can activate *Dspp* expression in vitro and partially rescue the root defects in *Gli1-Cre^{ERT2};Runx2^{fl/fl}* mice.

Discussion

During development, progenitor cells play crucial roles in organogenesis. It is therefore important to improve our understanding of the fate control of progenitor cells to advance developmental biology and regenerative medicine. Tooth root development has emerged as an excellent model to study how progenitor cells contribute to organogenesis at late developmental stages. In this study, we discovered that *Runx2*, a transcription factor well known for its role in the fate determination of pluripotent mesenchymal cells committing to the osteoblastic lineage, also defines the stem cell niche and regulates the fate of GLI1+ progenitor cells during tooth root development, partially through activating WNT inhibitor *NOTUM* expression in the preodontoblast region to trigger the odontoblastic lineage commitment of root progenitor cells. Our results suggest that *Runx2* is important in the cell fate determination of progenitor cells of different origins.

The *Runx2*-mediated regulatory network in controlling tooth development is complex. In early embryonic tooth development, FGF derived from the epithelium induces expression of *Runx2* in the dental mesenchyme, which in turn regulates the expression of mesenchymal *Fgf3* and other downstream targets. These downstream targets then induce *Shh* expression in the epithelial enamel knot to support crown formation.⁽³⁴⁾ *Runx2*-deficient mice exhibit arrested tooth development at the cap stage.⁽¹¹⁾ In postnatal stages of crown formation, *Runx2* expression is detectable in ameloblasts during the late secretory and maturation stages, and *Runx2* deficiency in ameloblasts results in enamel hypomineralization, a phenotype seen in CCD patients.⁽¹²⁾ *Runx2* expression is not present in HERS (see Fig. 1B,F), and loss of epithelial *Runx2* does not affect root elongation and dentin formation,⁽¹²⁾ suggesting that epithelial *Runx2* has little impact on the dental mesenchyme. Our study discovered that in tooth root development, *Runx2* expression overlaps with a subpopulation of GLI1+ cells in the dental mesenchyme, but they are not progenitor cells. Loss of *Runx2* in these GLI1+ cells and their progeny results in severe root developmental defects. We demonstrated that *Runx2* regulates odontoblast differentiation through a key downstream target, *NOTUM*, in the preodontoblast region of mouse molars, together with other downstream target genes, *Gli1*, *Pcp4*, and *Sfrp2*, to control the fate of root progenitor cells, thus supporting root formation. Our findings expand the understanding of the function of *Runx2* in regulating tooth development and help to elucidate how *Runx2* achieves functional specificity in regulating the development of diverse tissues and organs.

NOTUM deacylates WNTs to suppress signaling activity.⁽³²⁾ As a secreted WNT antagonist, it is crucial in several developmental processes, including vertebrate neural and head induction, bone formation, and tracheal cartilage patterning.^(33,35,36) *NOTUM* null mice develop dentin dysplasia and short tooth roots,⁽³⁷⁾ indicating that *NOTUM* functions in tooth root formation. Here, we first illustrated the expression pattern of *NOTUM* in the preodontoblast region during tooth root development and demonstrated that *Runx2* is an upstream regulator of *NOTUM*. NOTUM

deacylates WNT3a to attenuate WNT/ β -catenin signaling, and its expression overlaps with that of *Ainx2* in the developing trachea,⁽³⁶⁾ which is consistent with our findings that ablation of *Runx2* in developing mouse molars results in diminished *NOTUM* expression and enhanced WNT/ β -catenin signaling, which disturbs the balance between proliferation and differentiation in the apical dental mesenchyme, resulting in root defects. We also propose that NOTUM influences odontoblast differentiation by inactivating of WNT ligands WNT3a and WNT4, which are secreted by the dental epithelial structure HERS, thus acting as an important mediator in the epithelial-mesenchymal interaction during root development. Moreover, we found that NOTUM could activate expression of the odontoblast marker *Dspp* in vitro and partially rescue the root defects in *Gli1-Cre^{ERT2};Runx2^{fl/fl}* mice. These findings suggest that *NOTUM* is a key regulator of odontoblast differentiation.

The interaction between *Runx2* and WNT signaling pathways has long been studied. *Runx2* regulates osteogenic lineage commitment of suture mesenchymal cells through directly stimulating the expression of WNT signaling genes *Tcf7*, *Wnt10b*, and *Wnt1*.⁽³⁸⁾ Canonical WNT signaling enhances *Runx2* expression to promote osteogenesis through direct binding to the promoter of *Runx2* by TCF1/LEF1 high-mobility group transcription factors, downstream of β -catenin.^(39,40) WNT signaling must be properly regulated during odontogenesis. Inactivating β -catenin in odontoblasts produces molars with a complete absence of roots, due to the disruption of odontoblast differentiation.^(41,42) Overexpression of β -catenin in *OC-Cre* mice leads to shortened roots and excessive formation of dentin and cementum.^(43,44) However, it has remained unknown how WNT/ β -catenin signaling is regulated during odontoblast differentiation. Here for the first time we revealed the important function of the WNT inhibitor NOTUM in this process. We identified that *Runx2* regulates canonical WNT signaling through activating *NOTUM* in tooth root development, providing insight into the regulatory network that links *Runx2* and the WNT/ β -catenin signaling pathway.

Runx2 is also detectable in the periodontal ligament and alveolar bone (see Supplemental Fig. 2A–C), and we observed severe defects in periodontal tissue in our mutant mice as well, indicating that *Runx2* also regulates other downstream targets to support root development. *Sfrp2* is also a secreted WNT repressor that inhibits canonical WNT signaling by enhancing phosphorylation of β -catenin and downregulating *Axin2*.⁽⁴⁵⁾ It also enhances osteogenic differentiation of dental MSCs and helps maintain their survival in vitro. Here we found that *Sfrp2* was expressed in the most apical region of the dental papilla and follicle, but not in the preodontoblast region, suggesting that *Sfrp2* may not be a key regulator of odontoblast commitment in vivo, but it may still be crucial for the survival of dental MSCs, as well as for the formation of periodontal tissue. PCP4 is a calmodulin (CaM) regulator protein, and we found that it was expressed in the apical dental mesenchyme, suggesting it may be involved in cell fate determination within this tissue. CaM regulates various cellular functions, including the cell cycle, cell death, ion transport, and neurotransmission.⁽⁴⁶⁾ The exact functions of *Sfrp2* and *Pcp4* in regulating tooth root development require further investigation.

GLI1+ cells are a well-established MSC population in many murine tissues, including bone marrow,⁽⁴⁷⁾ molar and incisor teeth,^(8,48) and cranial sutures.⁽⁴⁹⁾ Nevertheless, they are heterogeneous. In our scRNA-seq data, we have shown that GLI1+ cells are distributed in different clusters, and we identified that RUNX2+ cells are a subpopulation of GLI1+ cells within the dental

mesenchyme. However, these cells do not contribute to root growth. Instead, these RUNX2+ cells appear to play an important role for the differentiation of preodontoblasts during root development. Moreover, loss of *Runx2* in GLI1+ MSCs results in a decrease of GLI1 signaling, suggesting that *Runx2* may be important for maintaining the stem cell niche in developing molars. It will be interesting to learn how these RUNX2+ cells provide feedback to regulate the stem cells. It also remains important for future research to define a more specific *in vivo* marker for MSCs in the developing tooth.

In summary, our study provides *in vivo* evidence of the crucial role of *Runx2* in regulating tooth root formation in a mouse model. This study improves our understanding of how *Runx2* regulates the development of diverse organs in a functionally specific manner. Moreover, we identified several unique downstream targets of *Runx2* in regulating root development, and we highlighted the function of a WNT inhibitor, NOTUM, in odontoblast differentiation. Our discovery yields new insights into the signaling network that regulates tooth root development and may have important implications for approaches to tooth regeneration.

Disclosures

The authors declare no conflicts of interest.

Acknowledgments

This study was supported by grants from the National Institute of Dental and Craniofacial Research, National Institutes of Health (RO1 DE022503 and RO1 DE025221). We thank Bridget Samuels and Linda Hattemer for critical reading of the manuscript. We acknowledge USC Libraries Bioinformatics Service for assisting with data analysis. The bioinformatics software and computing resources used in the analysis are funded by the USC Office of Research and the USC Libraries.

Authors' roles: QW and YC designed the study. QW performed most of the experiments, made all figures and analyzed the data. JJ, XH, and YY helped to analyze the NGS data. JF provided critical comments. YM and SC participated in sample collection and mouse surgery. T-VH participated in the μ CT analysis. QW and YC co-wrote the paper. YC supervised the research.

Author contributions: QW: Conceptualization; data curation; formal analysis; investigation; methodology; validation; visualization; writing-original draft; writing-review and editing. JJ: Formal analysis; methodology. XH: Formal analysis; methodology. JF: Conceptualization; methodology. YY: Formal analysis. YM: Investigation. SC: Investigation; resources. T-VH: Formal analysis. YC: Conceptualization; data curation; funding acquisition; methodology; resources; supervision; writing-original draft; writing-review and editing.

References

- Jernvall J, Thesleff I. Iterative signaling and patterning during mammalian tooth morphogenesis. *Mech Dev.* 2000;92(1):19–29.
- Chai Y, Jiang X, Ito Y, et al. Fate of the mammalian cranial neural crest during tooth and mandibular morphogenesis. *Development.* 2000;127(8):1671.
- Chai Y, Maxson RE Jr. Recent advances in craniofacial morphogenesis. *Dev Dyn.* 2006;235(9):2353–75.
- Tucker A, Sharpe P. The cutting-edge of mammalian development; how the embryo makes teeth. *Nat Rev Genet.* 2004;5(7):499–508.
- Thesleff I. Epithelial-mesenchymal signalling regulating tooth morphogenesis. *J Cell Sci.* 2003;116(Pt 9):1647–8.
- Li J, Parada C, Chai Y. Cellular and molecular mechanisms of tooth root development. *Development.* 2017;144(3):374–84.
- Ono W, Sakagami N, Nishimori S, Ono N, Kronenberg HM. Parathyroid hormone receptor signalling in osterix-expressing mesenchymal progenitors is essential for tooth root formation. *Nat Commun.* 2016;7:11277.
- Feng J, Jing J, Li J, et al. BMP signaling orchestrates a transcriptional network to control the fate of mesenchymal stem cells in mice. *Development.* 2017;144(14):2560–9.
- Komori T. Regulation of bone development and extracellular matrix protein genes by RUNX2. *Cell Tissue Res.* 2010;339(1):189–95.
- Mundlos S, Otto F, Mundlos C, et al. Mutations involving the transcription factor CBFA1 cause cleidocranial dysplasia. *Cell.* 1997;89(5):773–9.
- D'Souza RN, Aberg T, Gaikwad J, et al. *Cbfa1* is required for epithelial-mesenchymal interactions regulating tooth development in mice. *Development.* 1999;126(13):2911–20.
- Chu Q, Gao Y, Gao X, et al. Ablation of *Runx2* in ameloblasts suppresses enamel maturation in tooth development. *Sci Rep.* 2018;8(1):9594.
- Ahn S, Joyner AL. Dynamic changes in the response of cells to positive hedgehog signaling during mouse limb patterning. *Cell.* 2004;118(4):505–16.
- Madisen L, Zwingman TA, Sunkin SM, et al. A robust and high-throughput Cre reporting and characterization system for the whole mouse brain. *Nat Neurosci.* 2010;13(1):133–40.
- Takarada T, Hinoi E, Nakazato R, et al. An analysis of skeletal development in osteoblast-specific and chondrocyte-specific runt-related transcription factor-2 (*Runx2*) knockout mice. *J Bone Miner Res.* 2013;28(10):2064–9.
- Bai CB, Auerbach W, Lee JS, Stephen D, Joyner AL. *Gli2*, but not *Gli1*, is required for initial *Shh* signaling and ectopic activation of the *Shh* pathway. *Development.* 2002;129(20):4753–61.
- Chen J, Tu XL, Esen E, et al. WNT7B promotes bone formation in part through mTORC1. *PLoS Genet.* 2014;10(11):e1004145.
- Perl AK, Wert SE, Nagy A, Lobe CG, Whitsett JA. Early restriction of peripheral and proximal cell lineages during formation of the lung. *Proc Natl Acad Sci U S A.* 2002;99(16):10482–7.
- Lu Y, Xie Y, Zhang S, Dusevich V, Bonewald LF, Feng JQ. DMP1-targeted Cre expression in odontoblasts and osteocytes. *J Dent Res.* 2007;86(4):320–5.
- Livak KJ, Schmittgen TD. *Methods.* Vol. 25. San Diego, CA: 2001. Analysis of relative gene expression data using real-time quantitative PCR and the 2(-Delta Delta C(T)) Method; pp. 402–408.
- Spandidos A, Wang X, Wang H, Seed B. PrimerBank: a resource of human and mouse PCR primer pairs for gene expression detection and quantification. *Nucleic Acids Res.* 2009;38(Suppl_1):D792–9.
- Butler A, Hoffman P, Smibert P, Papalexis E, Satija R. Integrating single-cell transcriptomic data across different conditions, technologies, and species. *Nat Biotechnol.* 2018;36(5):411–20.
- Stuart T, Butler A, Hoffman P, et al. Comprehensive integration of single-cell data. *Cell.* 2019;177(7):1888–902.e21.
- Buenostro JD, Wu B, Chang HY, Greenleaf WJ. ATAC-seq: a method for assaying chromatin accessibility genome-wide. *Curr Protoc Mol Biol.* 2015;109:21.29.1–9.
- Heinz S, Benner C, Spann N, et al. Simple combinations of lineage-determining transcription factors prime cis-regulatory elements required for macrophage and B cell identities. *Mol Cell.* 2010;38(4):576–89.
- Lacerda-Pinheiro S, Dimitrova-Nakov S, Harichane Y, et al. Concomitant multipotent and unipotent dental pulp progenitors and their respective contribution to mineralised tissue formation. *Eur Cell Mater.* 2012;23:371–86.
- Camilleri S, McDonald F. *Runx2* and dental development. *Eur J Oral Sci.* 2006;114(5):361–73.
- Komori T, Yagi H, Nomura S, et al. Targeted disruption of *Cbfa1* results in a complete lack of bone formation owing to maturational arrest of osteoblasts. *Cell.* 1997;89(5):755–64.

29. Yamashiro T, Tummers M, Thesleff I. Expression of bone morphogenetic proteins and Msx genes during root formation. *J Dent Res*. 2003;82(3):172–6.
30. Zhao D, Vaziri Sani F, Nilsson J, et al. Expression of Pit2 sodium-phosphate cotransporter during murine odontogenesis is developmentally regulated. *Eur J Oral Sci*. 2006;114(6):517–23.
31. Takahashi A, Nagata M, Gupta A, et al. Autocrine regulation of mesenchymal progenitor cell fates orchestrates tooth eruption. *Proc Natl Acad Sci U S A*. 2019;116(2):575–80.
32. Kakugawa S, Langton PF, Zebisch M, et al. NOTUM deacylates Wnt proteins to suppress signalling activity. *Nature*. 2015;519(7542):187–92.
33. Zhang X, Cheong SM, Amado NG, et al. NOTUM is required for neural and head induction via Wnt deacylation, oxidation, and inactivation. *Dev Cell*. 2015;32(6):719–30.
34. Aberg T, Wang XP, Kim JH, et al. Runx2 mediates FGF signaling from epithelium to mesenchyme during tooth morphogenesis. *Dev Biol*. 2004;270(1):76–93.
35. Brommage R, Liu J, Vogel P, et al. NOTUM inhibition increases endocortical bone formation and bone strength. *Bone Res*. 2019;7(2).
36. Gerhardt B, Leesman L, Burra K, et al. NOTUM attenuates Wnt/beta-catenin signaling to promote tracheal cartilage patterning. *Dev Biol*. 2018;436(1):14–27.
37. Vogel P, Read RW, Hansen GM, et al. Dentin dysplasia in NOTUM knockout mice. *Vet Pathol*. 2016;53(4):853–62.
38. Qin X, Jiang Q, Miyazaki T, Komori T. Runx2 regulates cranial suture closure by inducing hedgehog, Fgf, Wnt, and Pthlh signaling pathway gene expression in suture mesenchymal cells. *Hum Mol Genet*. 2019;28(6):896–911.
39. Gaur T, Lengner CJ, Hovhannisyan H, et al. Canonical WNT signaling promotes osteogenesis by directly stimulating Runx2 gene expression. *J Biol Chem*. 2005;280(39):33132–40.
40. Dong YF, Soung DY, Schwarz EM, O’Keefe RJ, Drissi H. Wnt induction of chondrocyte hypertrophy through the Runx2 transcription factor. *J Cell Physiol*. 2006;208(1):77–86.
41. Kim TH, Bae CH, Lee JC, et al. β -Catenin is required in odontoblasts for tooth root formation. *J Dent Res*. 2013;92(3):215–21.
42. Zhang R, Yang G, Wu X, Xie J, Yang X, Li T. Disruption of Wnt/beta-catenin signaling in odontoblasts and cementoblasts arrests tooth root development in postnatal mouse teeth. *Int J Biol Sci*. 2013;9(3):228–36.
43. Bae CH, Lee JY, Kim TH, et al. Excessive Wnt/beta-catenin signaling disturbs tooth-root formation. *J Periodontol Res*. 2013;48(4):405–10.
44. Kim TH, Lee JY, Baek JA, et al. Constitutive stabilization of β -catenin in the dental mesenchyme leads to excessive dentin and cementum formation. *Biochem Biophys Res Commun*. 2011;412(4):549–55.
45. Jin L, Cao Y, Yu G, et al. SFRP2 enhances the osteogenic differentiation of apical papilla stem cells by antagonizing the canonical WNT pathway. *Cell Mol Biol Lett*. 2017;22:14.
46. Berchtold MW, Villalobo A. The many faces of calmodulin in cell proliferation, programmed cell death, autophagy, and cancer. *Biochim Biophys Acta*. 2014;1843(2):398–435.
47. Schneider RK, Mullally A, Dugourd A, et al. Gli1+ mesenchymal stromal cells are a key driver of bone marrow fibrosis and an important cellular therapeutic target. *Cell Stem Cell*. 2017;20(6):785–800.e8.
48. Zhao H, Feng J, Seidel K, et al. Secretion of shh by a neurovascular bundle niche supports mesenchymal stem cell homeostasis in the adult mouse incisor. *Cell Stem Cell*. 2014;14(2):160–73.
49. Zhao H, Feng J, Ho TV, Grimes W, Urata M, Chai Y. The suture provides a niche for mesenchymal stem cells of craniofacial bones. *Nat Cell Biol*. 2015;17(4):386–96.